DELFT UNIVERSITY OF TECHNOLOGY

REPORT 00-06

SEGREGATED SOLUTION METHODS FOR COMPRESSIBLE FLOW

D.R. VAN DER HEUL, C. VUIK AND P. WESSELING

Stability Analysis of
Segregated Solution Methods for Compressible Flow

D.R. van der Heul*, C. Vuik

P. Wesseling

J. M. Burgers Center and
Faculty of Information Technology and Systems
Department of Applied Mathematical Analysis
Delft University of Technology
Mekelweg 4 2628 CD Delft, The Netherlands

Abstract

A stability analysis is presented for staggered schemes for the governing equations of compressible flow. The method is based on Fourier analysis. The approximate nature of pressure-correction solution methods is taken into account.

1   Introduction

The aim of this paper is to describe a simple way of analyzing the stability properties of staggered schemes for the governing equations of compressible flow. These methods [1, 4, 6, 8, 11, 16, 18] are extensions of incompressible methods, that are able to handle weakly compressible flow with Mach $\downarrow$ 0 as well as fully compressible flow [1, 9]. Frequently, in this type of method the primitive variables are not updated collectively, but in some sequential order, as in fractional step methods. Such methods will be referred to as segregated solution methods. For the stability conditions of these schemes only heuristic arguments have been available, arising from the analysis of numerical schemes for a model scalar convection equation. Here we present a stability analysis based on Fourier analysis of the coupled system, that gives a prediction for the maximum allowable timestep for both (semi)-implicit and explicit methods as a function of the Mach number. The analysis can serve as a guideline for the development of new time integration schemes and solution procedures. The stability of the time stepping schemes can be influenced by choosing

---

different integration schemes for each equation as well as for different terms in each equation (IMEX-approach). The latter can lead to unexpected stability properties.

For the sake of brevity we present all results in only one spatial dimension. However, the results for the fully compressible case apply equally well to the multi-dimensional case, by considering the velocity componentwise.

The outline of the paper is as follows: In Section 2 we will consider a particular example of a segregated solution method for compressible fluid flow, that we use to illustrate our approach.

In Section 3 the application of the Homogeneous Equilibrium Model (HEM) for two-phase flow is briefly discussed. In the HEM the two-phase flow is modelled as a homogeneous mixture, with a spatially strongly varying speed of sound. The latter fact will cause the Mach number (Ma $\equiv u/c$, $u =$ velocity, $c =$ speed of sound) in the flow domain to vary from the incompressible limit Ma $= 0$ to the highly compressible values Ma $= 20 - 30$ and provides an excellent opportunity to test our predicted threshold on the CFL number (CFL $\equiv \sup(|u|)\delta t/\delta x$), CFL$_{\mathrm{max}} = f(\mathrm{Ma})$.

Section 4 describes our method for stability analysis. We start in Section 4.1 with a scheme for which the heuristic approach for stability analysis leads to incorrect predictions of the stability bounds. Next we treat this case to illustrate our method for stability analysis in Section 4.2. In Section 4.3 the more advanced case where the solution procedure is also incorporated in the analysis is considered.

In Section 5 a verification of these results is given for a number of testcases based on one-dimensional Riemann problems. For these cases the predicted bounds turn out to be very accurate.

2   Compressible pressure correction

In this paper we restrict ourselves to inviscid isothermal flow. The isothermal Euler equations are given by:

$$\frac{\partial \rho}{\partial t} + \frac{\partial m}{\partial x} = 0, \tag{1}$$
$$\frac{\partial m}{\partial t} + \frac{\partial}{\partial x}\left(um\right) = -\frac{\partial p}{\partial x}.$$

As opposed to methods based on flux-vector/flux-difference splitting or approximate Riemann solvers, here the equations are solved for sequentially. In the pressure correction method [1, 5, 10] the pressure is taken implicit in the momentum equation. This ensures that in the incompressible limit the scheme will reduce to the incompressible MAC-scheme, where the pressure acts as a Lagrangian multiplier to fulfill the solenoidality constraint on the velocity. In the case of high Mach number flow, it is not necessary to handle the pressure implicitly in the momentum equation. First a prediction is made of the momentum:

$$\frac{m^* - m^n}{\delta t} + \frac{\partial}{\partial x}\left(u^n m^*\right) = -\frac{\partial}{\partial x}p^n. \tag{2}$$

4

Next the following correction is postulated:

$$m^{n+1} \equiv m^* - \frac{\partial}{\partial x}\left(p^{n+1} - p^n\right) \equiv m^* - \frac{\partial}{\partial x}\delta p \tag{3}$$

and substituted in the mass-conservation equation to give the following pressure correction equation:

$$\frac{\rho(p^n + \delta p) - \rho^n}{\delta t} + \frac{\partial}{\partial x}\left(m^* - \frac{\partial p}{\partial x}\right) = 0. \tag{4}$$

3   Homogeneous Equilibrium Model

Our motivation for studying the method outlined above lies in its ability to handle the governing equations of the Homogeneous Equilibrium Model (HEM) very efficiently. The HEM is a simple model for two-phase liquid-vapor flow. Assuming thermodynamic equilibrium and neglecting velocity slip between both phases, it is possible to derive single phase equations for the two-phase mixture completed with a mixture equation of state. The equation of state $p = p(\rho)$ makes the density of the mixture equal to the density of the liquid phase when the pressure is above the vapor pressure, and equal to the density of the vapor phase below the vapor pressure, with a smooth, but artificial, transition in between. When the pressure of the mixture is either well below or above the vapor pressure, the speed of sound is large but finite and the flow is weakly compressible. In the phase transition region the speed of sound has a very small value of $\mathcal{O}(1\mathrm{m/s})$. In practical applications this means that the Mach number will vary from 0 to an artificial value well in the range of 10-30. For efficient computation of two-phase flow with the HEM it is therefore required
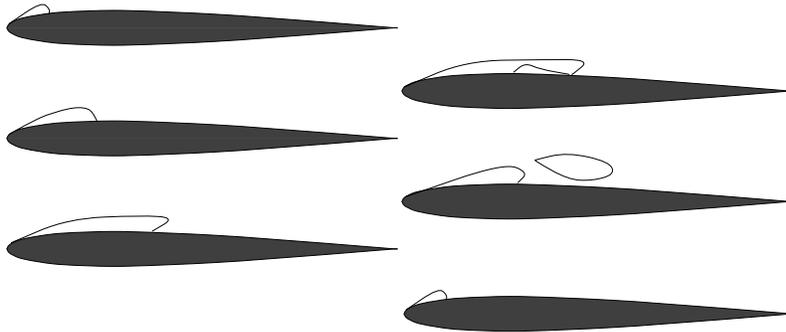
Figure 1: Cyclic behavior of unsteady sheet cavitation on hydrofoil.

that the time integration method is accurate and efficient uniformly in the Mach number for $0 < \mathrm{Ma} < 30$.

Supported by the following stability analysis method we have found it possible to derive a first order time integration scheme with almost unconditional stability for $0 < \mathrm{Ma} < 30$, but this scheme will not be discussed here.

The HEM has been applied to model unsteady sheet cavitation on hydrofoils in [2, 3, 7, 13, 14, 15, 17, 19]. This is a cyclic process involving periodic formation and shedding of thin vapor filled pockets on the suction side of hydrofoils, as illustrated in Figure 1. In each cycle, the cavity appears and grows to its maximum size. Meanwhile a re-entrant jet develops at the aft end of the cavity, that moves forward and upward as time progresses. At a certain instant the forward moving re-entrant jet touches the upper liquid/vapor interface, and the aft part of the cavitation bubble is shed. The cyclic behavior becomes periodic after a large number of cycles has been completed. To bridge this initial phase efficiently a time integration scheme is required, that allows for large time steps .

4   Stability analysis

First we show how a heuristic approach fails to predict the stability condition for a simple scheme. Next an improved stability analysis is formulated and applied to the latter scheme and to one with a more advanced spatial discretisation and solution procedure. For brevity we restrict ourselves to isothermal flow, but inclusion of an energy equation in the analysis is straightforward.

4.1   Breakdown of heuristic approach

We start with an example that shows how a heuristic approach fails to predict stability of the time integration method. We consider the following discretised version of (1):

$$\frac{\rho_j^{n+1} - \rho_j^n}{\delta t} + \frac{1}{\delta x}\left(\frac{\rho_j^{n+1}}{\frac{1}{2}\left(\rho_{j+1}^{n+1} + \rho_j^{n+1}\right)}m_{j+\frac{1}{2}}^{n+1} - \frac{\rho_{j-1}^{n+1}}{\frac{1}{2}\left(\rho_j^{n+1} + \rho_{j-1}^{n+1}\right)}m_{j-\frac{1}{2}}^{n+1}\right) = 0, \qquad (5)$$

$$\frac{m_{j+\frac{1}{2}}^{n+1} - m_{j+\frac{1}{2}}^n}{\delta t} + \frac{1}{\delta x}\left(u_{j+\frac{1}{2}}^n m_{j+\frac{1}{2}}^n - u_{j-\frac{1}{2}}^n m_{j-\frac{1}{2}}^n\right) = -\frac{1}{\delta x}\left(p_{j+1}^{n+1} - p_j^{n+1}\right).$$

Note the following features:

- staggering of momentum m with respect to the scalar unknowns ρ and p (Figure 2),

- spatial discretisation of the convective terms in the momentum equation is first order upwind, whereas the pressure gradient is centrally discretised,

- application of first order density upwind bias [1] in the mass conservation equation,

- explicit discretisation of the convective term in the momentum equation, which removes the splitting error, encountered in fully implicit pressure correction.

An heuristic approach to analyze the stability of this system is to look at the convection equation for a scalar ϕ:

$$\phi_t = -a\phi_x, \qquad (6)$$
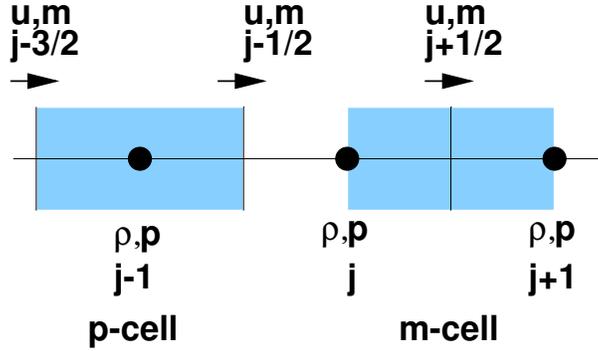
Figure 2: Staggered placement of unknowns

with the convection velocity a taken equal to the maximum signal speed of the isothermal Euler equations, $|u| + c$, where u is the fluid velocity and c is the speed of sound, defined as $\left(\frac{d\rho}{dp}\right)^{-\frac{1}{2}}$. Either by Schur-Cohn theory or by the approach of [20] it is possible to analyze the stability for various spatial and temporal discretisations. For a first order upwind discretisation, the implicit Euler method is unconditionally stable, and the explicit Euler method is stable under the following condition:

$$\frac{\sup(|u| + c)\delta t}{\delta x} < 1 \Leftrightarrow \frac{\sup(|u|)(1 + \text{Ma}^{-1})\delta t}{\delta x} < 1, \tag{7}$$

or

$$\text{CFL} \equiv \frac{\sup(|u|)\delta t}{\delta x} \leq \frac{1}{1 + \text{Ma}^{-1}} = \frac{\text{Ma}}{1 + \text{Ma}}. \tag{8}$$

Practical experience shows that this gives a useful indication for stability of colocated schemes that use explicit Euler time stepping. Note that we do not use the more common definition $\text{CFL} = \sup(|u| + c)\delta t/\delta x$.

The scheme under consideration uses a mixture of implicit and explicit Euler timestepping, and therefore one might think that a conservative estimate of the maximum allowable timestep could be made based on (8). However, numerical experiments for high Mach number Riemann problems revealed that the scheme is stable only if the CFL number is taken much smaller than required by (8), and that the maximum allowable CFL number decreases with increasing Mach number. This example illustrates, that the stability properties of a system cannot be deduced in a simple manner from those of a scheme for a single equation, when a staggered scheme is used. A more sophisticated stability analysis is needed, that is able to handle different time integration schemes for the individual equations.

4.2 Fourier stability analysis; case 1

We start our analysis by reformulating the discretised system in the two variables m and ρ. To make Fourier analysis possible we assume a linear equation of state:

$$\rho = c^{-2}p.$$

A perturbed solution is postulated:

$$\begin{pmatrix} \rho_j + \delta\rho_j \\ m_j + \delta m_j \end{pmatrix}$$

and substituted in the discretised system (5). Next the system is linearized. This leaves us with the following system for the perturbations:

$$\frac{\delta\rho_j^{n+1} - \delta\rho_j^n}{\delta t} + \frac{1}{\delta x}\left[\left(\delta m_{j+\frac{1}{2}}^{n+1} + u_{j+\frac{1}{2}}^{n+1}\left(\delta\rho_j^{n+1} - \delta\rho_{j+1}^{n+1}\right)\right) - \left(\delta m_{j-\frac{1}{2}}^{n+1} + u_{j-\frac{1}{2}}^{n+1}\left(\delta\rho_{j-1}^{n+1} - \delta\rho_j^{n+1}\right)\right)\right] = 0,$$

$$\frac{\delta m_{j+\frac{1}{2}}^{n+1} - \delta m_{j+\frac{1}{2}}^n}{\delta t} + \frac{1}{\delta x}\left[\left(2u_{j+\frac{1}{2}}^n \delta m_{j+\frac{1}{2}}^n - \left(u_{j+\frac{1}{2}}^n\right)^2 \delta\rho_{j+\frac{1}{2}}^n\right) - \left(2u_{j-\frac{1}{2}}^n \delta m_{j-\frac{1}{2}}^n - \left(u_{j-\frac{1}{2}}^n\right)^2 \delta\rho_{j-\frac{1}{2}}^n\right)\right] = -\frac{1}{\delta x}c^2\left(\delta\rho_{j+1}^{n+1} - \delta\rho_j^{n+1}\right),$$

where we have written:

$$u_{j+\frac{1}{2}} \equiv \frac{2m_{j+\frac{1}{2}}}{\rho_j + \rho_{j+1}}.$$

In order to apply Fourier analysis to the "frozen coefficients" case we put $u_{j+\frac{1}{2}}^{n+1} = U = $ constant and obtain (dropping the increment notation):

$$\frac{\rho_j^{n+1} - \rho_j^n}{\delta t} + \frac{1}{\delta x}\left[\left(m_{j+\frac{1}{2}}^{n+1} - m_{j-\frac{1}{2}}^{n+1}\right) + \frac{1}{2}U\left(-\rho_{j-1}^{n+1} + 2\rho_j^{n+1} - \rho_j^{n+1}\right)\right] = 0,$$

$$\frac{m_{j+\frac{1}{2}}^{n+1} - m_{j+\frac{1}{2}}^n}{\delta t} + \frac{1}{\delta x}\left[\left(2Um_{j+\frac{1}{2}}^n - U^2\left(\frac{\rho_{j+1}^n}{2}\right)\right) - \left(2Um_{j-\frac{1}{2}}^n - U^2\left(\frac{\rho_{j-1}^n}{2}\right)\right)\right] + \frac{1}{\delta x}c^2\left(\rho_{j+1}^{n+1} - \rho_j^{n+1}\right) = 0.$$

If the perturbations are postulated to have the following form:

$$\begin{pmatrix} \rho_j^n \\ m_j^n \end{pmatrix} = \begin{pmatrix} \tilde{\rho}^n \\ \tilde{m}^n \end{pmatrix} e^{ij\theta},$$

8

the system can be written as :

$$
\begin{bmatrix} 1 + \frac{U\delta t}{\delta x}(1 - \cos(\theta)) & \frac{2\delta t}{\delta x}i\sin(\theta/2) \\ \frac{2c^2\delta t}{\delta x}i\sin(\theta/2) & 1 \end{bmatrix} \begin{pmatrix} \tilde{\rho}^{n+1} \\ \tilde{m}^{n+1} \end{pmatrix} =
$$

$$
\begin{bmatrix} 1 & 0 \\ \frac{U^2\delta t}{2\delta x}i\sin(\theta)e^{-\frac{1}{2}i\theta} & 1 - \frac{4U\delta t}{\delta x}i\sin(\theta/2)e^{-\frac{1}{2}i\theta} \end{bmatrix} \begin{pmatrix} \tilde{\rho}^n \\ \tilde{m}^n \end{pmatrix},
$$

or in brief

$$
G_2 \begin{pmatrix} \tilde{\rho}^{n+1} \\ \tilde{m}^{n+1} \end{pmatrix} = G1 \begin{pmatrix} \tilde{\rho}^n \\ \tilde{m}^n \end{pmatrix}.
$$

The amplification matrix of the system is $G_2^{-1}G_1$. The scheme is *Von Neumann stable* if:

$$
|\lambda_{1,2}(G_2^{-1}G_1)| \leq 1.
$$

Note that $\lambda_{1,2}$ solve the equation

$$
\det(G_1 - \lambda G_2) = 0,
$$

which leads to :

$$
\lambda_{1,2} = \frac{1}{2((1+b) - a^2c^2)}[2 - 2(1+b)ag - ak + b\pm \tag{9}
$$
$$
\left(4(1+b)^2 a^2g^2 - 4b(1+b)ag + 4a^2kg(1+b) - 4ak\right.
$$
$$
\left. + b^2 - 2abk + a^2k^2 + 4a^2c^2 - 8a^3gc^2\right)^{\frac{1}{2}}],
$$

where

$$
\begin{array}{llll}
a & = & \frac{2\delta t}{\delta x}i\sin(\theta/2), & g & = & Ue^{-\frac{1}{2}i\theta}, \\
b & = & \frac{U\delta t}{\delta x}(1 - \cos(\theta)), & k & = & \frac{U^2\delta t}{\delta x}i\sin(\theta)e^{-\frac{1}{2}i\theta}.
\end{array}
$$

Figures 3(a) and 3(b) show graphs of $|\lambda_{1,2}|$ as a function of θ. If both U, $\frac{\delta t}{\delta x}$ and c are systematically varied we find numerically that in all cases the graph is an even function of θ and that a local extremum occurs for $\theta = 0$. As consistency requires that for $\theta = 0$, $\lambda_{1,2}(G_2^{-1}G_1) = 1$, the occurrence of a local minimum for $\theta = 0$ means that in the neighborhood of $\theta = 0$, $|\lambda_{1,2}(G_2^{-1}G_1)|$ will exceed unity and the integration will be unstable.

Based on this argument we can formulate the following necessary, but not sufficient condition for stability:

$$
\exists \varepsilon > 0 \mid \forall \theta \in \langle -\varepsilon, \varepsilon \rangle \backslash \{0\} : \frac{d^2|\lambda_{1,2}|}{d\theta^2} < 0. \tag{10}
$$

Expansion for $|\theta| << 1$ gives

$$
\lambda_{1,2}\overline{\lambda}_{1,2} = 1 + b_{1,2}\theta + c_{1,2}\theta^2 + O(\theta^3).
$$

(a) Case of instability.

(b) Case of stability.
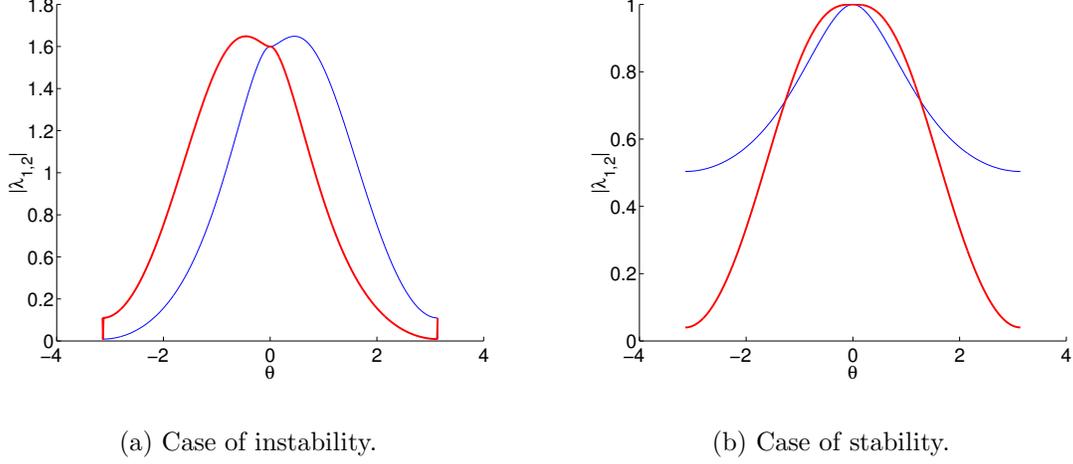
Figure 3: Dependence of $|\lambda_{1,2}(G_2^{-1}G_1)|$ on θ.

Because $b_{1,2} = 0$, obviously, a necessary but not sufficient condition for stability is:

$$(c_{1,2}) \leq 0,$$

or

$$\left(4 - \frac{2}{\text{Ma}^2} \pm 2\text{Ma}\right)\frac{U\delta t}{\delta x} \leq 3, \tag{11}$$

which should be fullfilled for both the $+$ and $-$ sign. If the Mach number is in the range $0.5 < \text{Ma} < 1.5$ we found that, although the eigenvalues are in the unit circle for $|\theta| < \epsilon$, $|\lambda_{1,2}|$ can exceed unity for $\theta = \pm\pi$. For this an additional constraint can be formulated:

$$\lambda_i \overline{\lambda_i}\big|_{\theta=\pm\pi} < 1$$

which leads to the following conditions:

$$\frac{U\delta t}{\delta x} < \frac{\text{Ma}^2 - \text{Ma}^2\sqrt{9 - \frac{4}{\text{Ma}^2}}}{1 - 2\text{Ma}^2}, \frac{2}{3} < \text{Ma}, \quad \text{or} \tag{12}$$

$$\frac{U\delta t}{\delta x} > \frac{\text{Ma}^2 + \text{Ma}^2\sqrt{9 - \frac{4}{\text{Ma}^2}}}{1 - 2\text{Ma}^2}, \frac{2}{3} < \text{Ma}.$$

For the case without density bias we can similarly derive from (10):

$$\left(4 - \frac{2}{\text{Ma}^2} \pm 2\text{Ma}\right)\frac{U\delta t}{\delta x} \leq 2 \pm \text{Ma}, \tag{13}$$

10
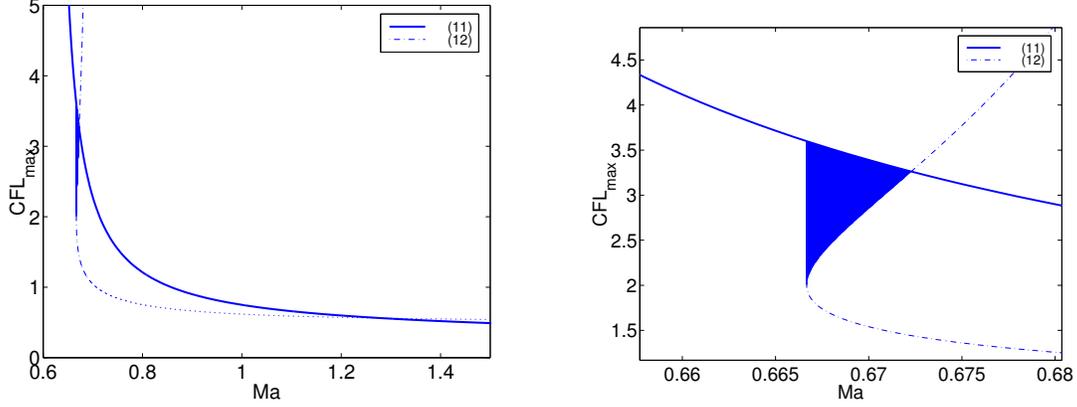
(a) Stability conditions (11) and (12).

(b) Zoom of 4(a).

Figure 4: Stability conditions for (5).

together with:

$$
\begin{aligned}
\frac{U\delta t}{\delta x} &< \mathrm{Ma}^2 + \mathrm{Ma}^2\sqrt{1 - \frac{1}{\mathrm{Ma}^2}}, 1 < \mathrm{Ma}, \quad \text{or} \\
\frac{U\delta t}{\delta x} &> \mathrm{Ma}^2 - \mathrm{Ma}^2\sqrt{1 - \frac{1}{\mathrm{Ma}^2}}, 1 < \mathrm{Ma}.
\end{aligned}
\tag{14}
$$

Taking the limit $\mathrm{Ma} \downarrow 0$ in (11) or (13), one finds unconditional stability. However, this stability prediction does not carry over to the multi-dimensional case. The one-dimensional case is special, because in the incompressible limit the mass conservation reduces to the solenoidality constraint, which in one spatial dimension means:

$$
\frac{\partial m}{\partial x} = 0 \Rightarrow m = m(t),
\tag{15}
$$

and this means that the momentumfield is fully represented by the Fourier mode $\theta = 0$. For a consistent discretisation the amplification factor of the zeroth order mode is unity by definition, and therefore the scheme is unconditionally stable. However, the multi-dimensional equivalent of (15)

$$
\mathrm{div}\ \mathbf{m} = 0,
$$

does have a nontrivial solution, a solenoidal vector field, and the previous argument no longer holds. In the multi-dimensional case we find indeed experimentally that for very small Mach numbers the scheme is not unconditionally stable. But practical experience shows that for $\mathrm{Ma} \cong 0.3$ the above necessary stability conditions give good predictions of

11
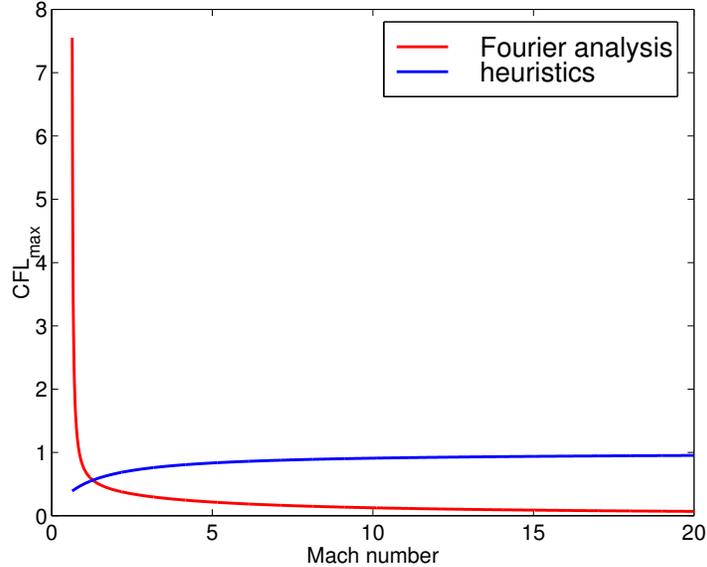
Figure 5: Stability conditions for (5).

the stability properties in the multi-dimensional case, if the above conditions are applied on a component-by-component basis.

In Figure 4(a) the two conditions (11) and (12) are shown. The integration will be stable if the CFL-number is chosen below curve (11) and curve (12). However, an additional region of stability exist between curves (11) and (12), shown as the black region in Figure 4(b). This additional region is of course of no practical interest.

Figure 5 shows the maximum allowable CFL number based on the heuristic prediction (11) and the one following from the present Fourier analysis of the system. It is clear that only for Ma < 1.3 the heuristic approach gives a conservative estimate of the maximum allowable CFL number, but that for Ma > 1.3 the heuristic condition is much weaker than (11). In Section 5 we will confirm the necessity of stability threshold (11), by a number of numerical experiments.

To show the general applicability of the stability analysis we analyzed the following four variants of scheme (5):either with an explicit or an implicit discretisation of the convective terms in the momentum equation and either with or without the density upwind bias in the mass conservation equation. For these four schemes the calculated upper and lower bounds on the CFL-number for two different Mach numbers are summarized in Table 1.

Note:

- For scheme 1 and Ma = 4 both an upper and a lower bound on the CFL-number should be satisfied, which is impractical.

- Although scheme 2 is more diffusive than scheme 1, due to the density upwind bias, the former is actually stable for a smaller CFL-number than the latter for Ma = 4.

12

scheme	momentum convection	density upwind bias	Ma = 4	Ma = 20
1	explicit	no	$0.485 < \mathrm{CFL} < 0.505$	uncond. unstable
2	explicit	yes	$\mathrm{CFL} < 0.253$	$\mathrm{CFL} < 0.068$
3	implicit	no	uncond. unstable	uncond. unstable
4	implicit	yes	$\mathrm{CFL} < 3.315$	$\mathrm{CFL} < 2.1$

Table 1: Stability properties of four variants of (5)

- Only schemes 2 and 4 can be used for practical computations.

- Although scheme 3 is discretised more implicitly than scheme 1, the latter actually has a stability window, whereas the former has not.

- By implicitly discretising the convective terms in the momentum equation, we can raise the stability bound by a factor 10 or more. Moreover, the dependence of the stability on Ma of the implicit scheme is much weaker than for the explicit case.

- The CFL-number threshold for scheme 4 of $\mathcal{O}(2)$, is what one would expect for an explicit scheme, not for an almost fully implicit scheme.

We will check the anomalous behavior of schemes 1 and 3, and the stability bound for scheme 4, for the case of Ma = 4 in Section 5.

4.3 Fourier stability analysis: case 2

If the convective terms in the momentum equation are discretised implicitly, the pressure correction formulation will no longer be identical to the original scheme. This is due to the fact that in the postulated momentum correction, the difference between the convective terms in the momentum predictor equation and the discretised momentum equation is neglected. We distinguish between the *target*, *actual* and *resolved* discretisation. The *target* discretisation is obtained after finite volume discretisation, can be nonlinear, and can only be solved for in an iterative manner. The *actual* discretisation follows from the *target* discretisation after linearisation, and the introduction of further approximations, such as deferred or defect correction. Finally, the *resolved* discretisation includes the segregated (pressure correction) solution procedure. The stability properties of *target* and *resolved* discretisation can differ considerably. Figure 6 shows the dependence of $|\lambda_{1,2}(G_2^{-1}G_1)|$ on θ, for the fully implicit version of (5), both with and without inclusion of the pressure correction algorithm. The different behavior of *resolved* and *target* discretisation as observed in Figure 6 shows that it is essential to study the stability properties of the resolved discretisation to make a correct estimate of the stability thresholds.

In the second case we will discuss, we include the pressure correction method in the stability analysis together with the necessary deferred correction steps, required to obtain a high order spatial discretisation on a compact stencil. The solution procedure is now as

13
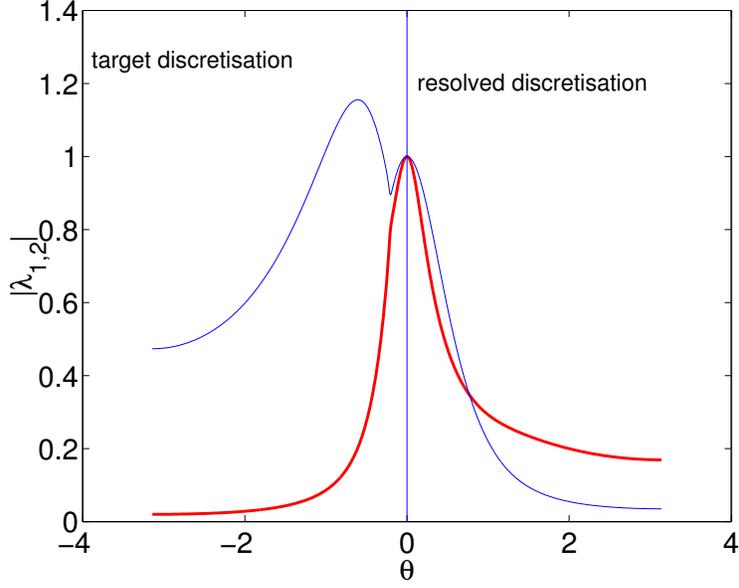
Figure 6: Dependence of $|\lambda_{1,2}(G_2^{-1}G_1)|$ on θ, with and without inclusion of the pressure correction algorithm.

follows: First the momentum predictor equation is solved with the $\kappa-$scheme in a deferred correction manner:

$$\frac{m^*_{j+\frac{1}{2}} - m^n_{j+\frac{1}{2}}}{\delta t} + \frac{1}{\delta x}\left(F_{j+1} - F_j\right) = -\frac{1}{\delta x}\left(p^n_{j+1} - p^n_j\right),$$
$$F_{j+1} = u^n_{j+\frac{1}{2}}m^*_{j+\frac{1}{2}} - u^n_{j+\frac{1}{2}}m^n_{j+\frac{1}{2}} +$$
$$\left(\frac{\kappa - 1}{4}u^n_{j-\frac{1}{2}}m^n_{j-\frac{1}{2}} + \frac{4 - 2\kappa}{4}u^n_{j+\frac{1}{2}}m^n_{j+\frac{1}{2}} + \frac{\kappa + 1}{4}u^n_{j+\frac{3}{2}}m^n_{j+\frac{3}{2}}\right).$$

Application of the $\kappa-$scheme to the mass conservation equation in (5) in a deferred

correction manner leads, after linearisation, to the following pressure correction equation:

$$\frac{\rho_j^{n+1} - \rho_j^n}{\delta t} + \frac{1}{\delta x}\left(G_{j+\frac{1}{2}} - G_{j-\frac{1}{2}}\right) = 0,$$

$$G_{j+\frac{1}{2}} = \sigma_{j+1/2,\text{HO}}^n m_{j+1/2}^* +$$

$$\left(\frac{\delta x}{4\rho^2 c^2}\frac{\partial p}{\partial x}|m^*|\right)_{j+1/2}\left(\left(\frac{d\rho}{dp}\right)_j \delta p_j + \left(\frac{d\rho}{dp}\right)_{j+1} \delta p_{j+1}\right) +$$

$$\left(-\frac{1}{2\rho}|m^*|\right)_{j+1/2}\left(\left(\frac{d\rho}{dp}\right)_{j+1} \delta p_{j+1} - \left(\frac{d\rho}{dp}\right)_j \delta p_j\right) - \sigma_{j+1/2,HO}^n\frac{\delta t}{\Delta x}\left(\delta p_{j+1} - \delta p_j\right)$$

$$+ \left(\frac{(\sigma_{\text{LO}}^n - \sigma_{\text{HO}}^n)\, m^*}{2\rho^n}\right)_{j+1/2}\left(\left(\frac{d\rho}{dp}\right)_{j+1} \delta p_{j+1} + \left(\frac{d\rho}{dp}\right)_j \delta p_j\right),$$

where

$$\sigma_{j+\frac{1}{2},\text{HO}}^n = \frac{2\left(\frac{\kappa-1}{4}\rho_{j-1}^n + \frac{4-2\kappa}{4}\rho_j^n + \frac{\kappa+1}{4}\rho_{j+1}^n\right)}{\rho_j^n + \rho_{j+1}^n},$$

$$\sigma_{j+\frac{1}{2},\text{LO}}^n = \frac{2\rho_j^n}{\rho_j^n + \rho_{j+1}^n}.$$

Application of the Fourier analysis procedure described in Section 4.2 leads to the following system of equations:
Predictor step

$$\begin{pmatrix} 1 & 0 \\ 0 & 1 + ag \end{pmatrix}\begin{pmatrix} \hat{\rho}^* \\ \hat{m}^* \end{pmatrix} = \begin{pmatrix} 1 & 0 \\ -q - ac^2 & 1 + ag - p \end{pmatrix}\begin{pmatrix} \hat{\rho}^n \\ \hat{m}^n \end{pmatrix},$$

Corrector step

$$\begin{pmatrix} 1 + ag - l + s & 0 \\ ac^2 & 1 \end{pmatrix}\begin{pmatrix} \hat{\rho}^{n+1} \\ \hat{m}^{n+1} \end{pmatrix} =$$

$$\begin{pmatrix} 1 + s & 0 \\ ac^2 & 0 \end{pmatrix}\begin{pmatrix} \hat{\rho}^n \\ \hat{m}^n \end{pmatrix} + \begin{pmatrix} ag - \frac{1}{2}p & -a \\ 0 & 1 \end{pmatrix}\begin{pmatrix} \hat{\rho}^* \\ \hat{m}^* \end{pmatrix},$$

where we have introduced the following abbreviations:

$$s = 1 - 2\cos(\theta), \qquad p = \frac{1}{4}U\lambda\left(e^{-2i\theta} - 7e^{-i\theta} + 3 + 3e^{i\theta}\right), \qquad l = U\lambda i\sin(\theta),$$

$$q = \frac{1}{16}U^2\lambda\hat{\rho}^{n+1}\left(-e^{-2\frac{1}{2}i\theta} + 6e^{-1\frac{1}{2}i\theta} + 4e^{-\frac{1}{2}i\theta} - 6e^{\frac{1}{2}i\theta} - 3e^{1\frac{1}{2}i\theta}\right).$$

Or in operator form:
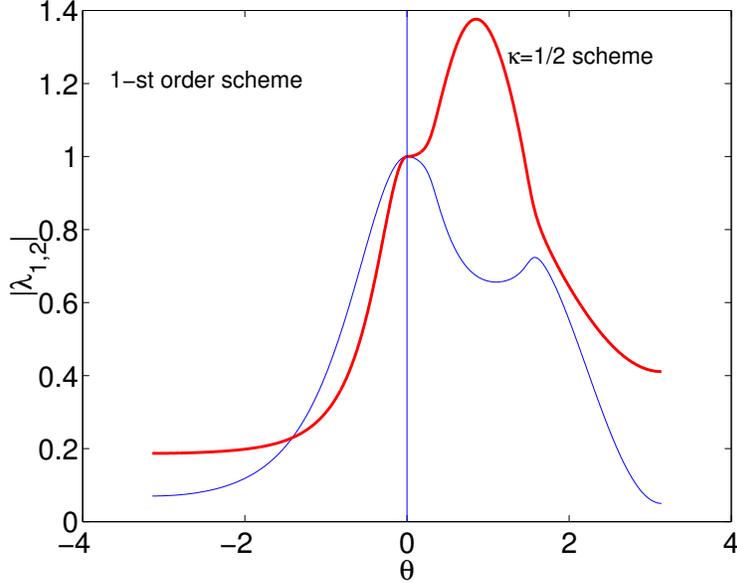
Figure 7: Dependence of $|\lambda_{1,2}(G_2^{-1}G_1)|$ on θ, for 1st-order upwind scheme with and without higher order upwind deferred correction.

$$G_1 \begin{pmatrix} \tilde{\rho}^* \\ \tilde{m}^* \end{pmatrix} = G_0 \begin{pmatrix} \tilde{\rho}^n \\ \tilde{m}^n \end{pmatrix},$$

$$G_4 \begin{pmatrix} \tilde{\rho}^{n+1} \\ \tilde{m}^{n+1} \end{pmatrix} = G_3 \begin{pmatrix} \tilde{\rho}^n \\ \tilde{m}^n \end{pmatrix} + G_2 \begin{pmatrix} \tilde{\rho}^* \\ \tilde{m}^* \end{pmatrix}.$$

The amplification matrix is now given by:

$$G_4^{-1} \left(G_3 + G_2 G_1^{-1} G_0 \right).$$

For stability we require that

$$|\lambda_{1,2}(G_4^{-1} \left(G_3 + G_2 G_1^{-1} G_0 \right))| \leq 1.$$

We have not succeeded yet in deriving from this simple necessary stability conditions, as in the first case. Instead, we compute $|\lambda_{1,2}(\theta)|$ for a sufficiently fine distribution of $-\pi < \theta < \pi$. For a scalar convection diffusion equation, we know [12] that stability is not affected by a deferred correction step. Figure 7 shows, however, that in the case of a system the functional dependence of $|\lambda_{1,2}|$ on θ is qualitatively different from that for the first order upwind scheme. Generally the CFL-number threshold for the higher order upwind scheme is much smaller than for the first order upwind scheme.

16

5 Verification of stability thresholds

We will first verify experimentally the stability conditions (11) and (12) for a number of testcases with increasing Mach-number. The testcase is a one-dimensional isothermal Riemann problem, with the initial states sufficiently close together. This means we can regard the solution of the Riemann problem as a small but structured perturbation of the initial constant state. The initial conditions are chosen in such a way that the velocity remains bounded by the initial left and right states.

Mach-number	CFL-number			
	stable	predicted(11),(12) present approach	predicted(8) heuristic approach	unstable
0.1	4.000	∞	0.009	—
1	0.600	0.618	0.500	0.650
5	0.200	0.215	0.833	0.250
10	0.080	0.125	0.909	0.170
15	0.060	0.088	0.938	0.100

Table 2: Numerical verification of the stability thresholds (11) and (12).

Table 2 shows the predicted threshold for the CFL number together with the smallest CFL number tested that induced instability and the largest CFL number tested that preserved stability for a range of Mach numbers. It is clear that the predicted stability threshold is very accurate. For the case Ma=1, use is made of the additional condition (12).

Figure 8 and Figure 9 show results for the testcase Ma = 5. At the start of the computation stability is dominated by nonlinear effects due to the discontinuous initial condition. An initial overshoot is created, but when the CFL number is chosen within the stability limits, it is eventually damped out.

Next we will verify experimentally the stability thresholds for the schemes presented in Table 1 in Section 4.2 for a testcase with Ma ≈ 4. First we choose scheme 1, for which both an upper and a lower bound on the CFL-number should be fullfilled. Figure 10 shows results for CFL = 0.43 chosen slightly smaller than the lower bound. The wiggles are clearly amplified. Next we choose CFL = 0.493, halfway between the upper and lower bound. Although wiggles occur during the startup phase, they are clearly damped out in time (Figure 11).

Next scheme 3 is used, with the same CFL = 0.493. Although this scheme is more implicit than Scheme 1, Figure 12 shows that the integration is unstable, in complete agreement with our analysis! Finally we will verify the stability threshold for scheme 4. Figure 13 shows a computation with CFL = 3.19, and Figure 14 with CFL = 3.61. In the first case the solution remains stable, whereas in the second case a smooth wiggle is formed. The smoothness of this overshoot is due to the fact that the absolute value of the
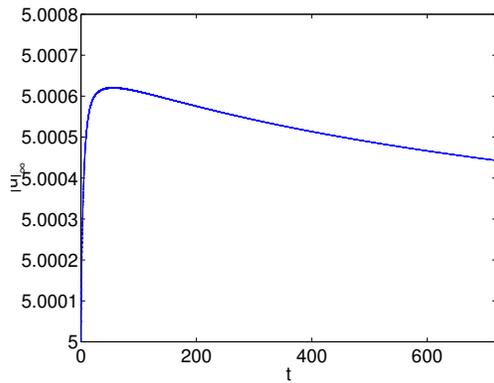
(a) $|\underline{u}|_\infty$ as function of time.
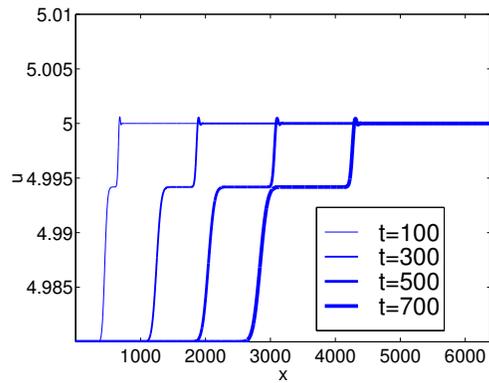
(b) Solution u at t=100, t=300, t=500 and t=700.

Figure 8: Stable integration of Ma = 5 testcase, CFL = 0.20.
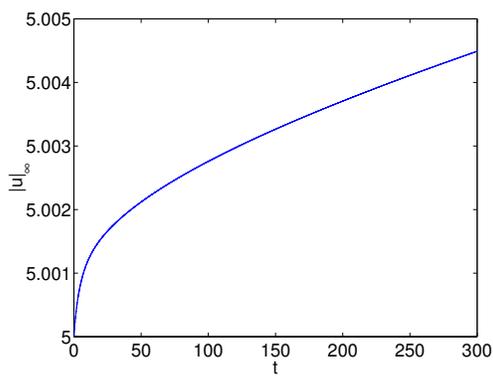
(a) $|\underline{u}|_\infty$ as function of time.
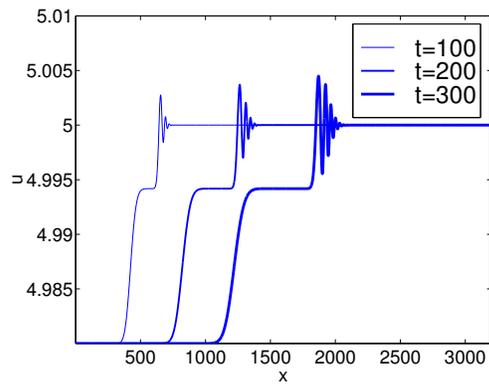
(b) Solution u at t=100, t=200 and t=300.

Figure 9: Unstable integration of Ma = 5 testcase, CFL = 0.25.
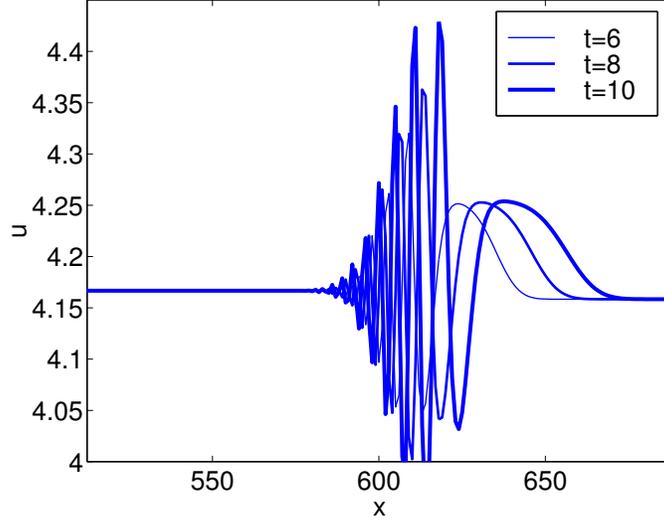
Figure 10: Unstable integration with scheme 1, CFL = 0.430.
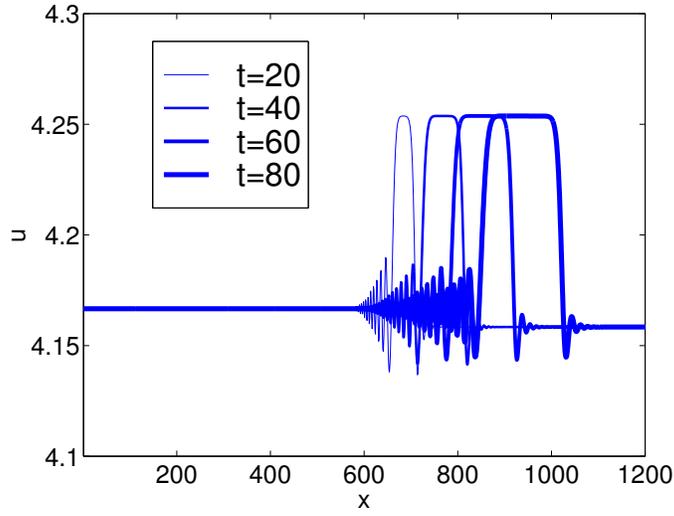
Figure 11: Stable integration with scheme 1, CFL = 0.493.

19
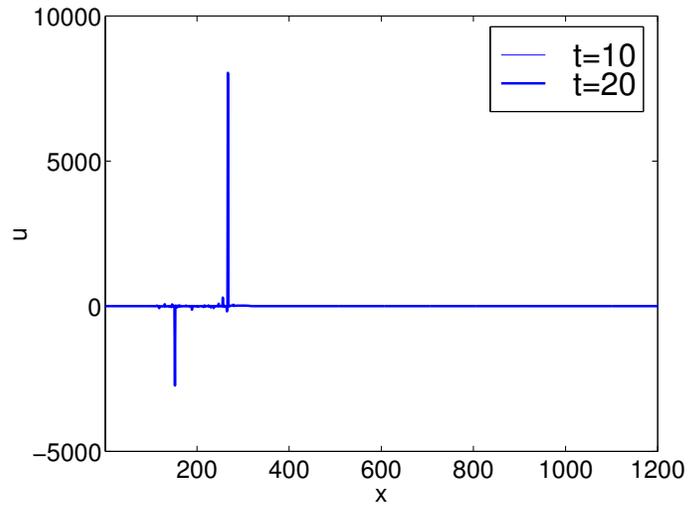
Figure 12: Unstable integration with scheme 3, CFL = 0.493.
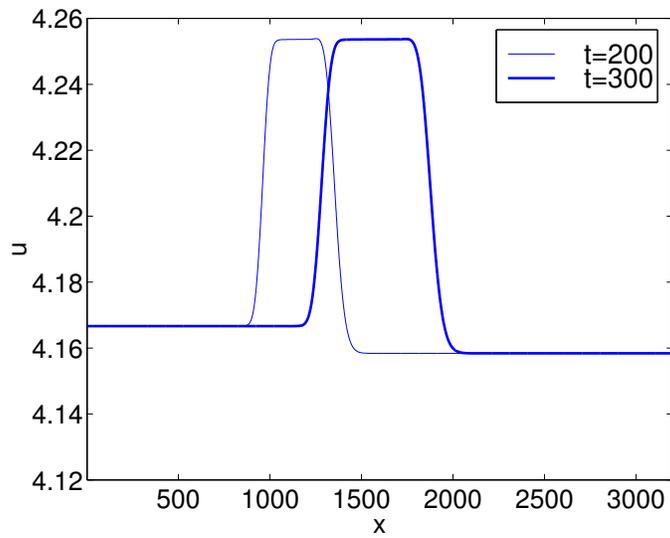
Figure 13: Stable integration with scheme 4, CFL = 3.19.

20
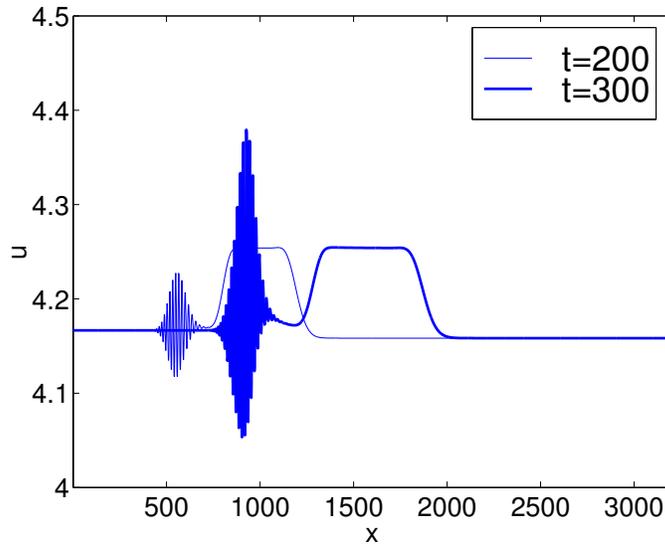
Figure 14: Unstable integration with scheme 4, CFL = 3.61.

eigenvalues of the amplification matrix exceeds unity in the low frequency domain, near $\theta = 0$. Of course only the schemes with density bias can be used for practical computations.

6   Conclusions and Future Extensions

Stability conditions based on heuristic extension of stability results for a scalar model problem are found not to be generally valid for segregated solution procedures. Therefore a more refined method of analysis is used, in which it is possible to include the details of the sequential solution procedure, and different time integration schemes for the individual equations. A number of numerical experiments support the derived stability thresholds.

We note that among the schemes considered only the last scheme discussed in Section 5 has reasonable stability properties, and that only for moderate Mach numbers. But with our stability analysis method we can optimize the scheme, to obtain a solution method, with unconditional stability and accuracy uniform in the Mach number, with special interest for efficient computations with the HEM.

References

[1] H. Bijl and P. Wesseling. A unified method for computing incompressible and compressible flows in boundary fitted coordinates. *Journal of Computational Physics*, 141:153–173, 1998.

[2] Y. Dellanoy and J.L. Kueny. Two phase flow approach in unsteady cavitation modelling. In *Cavitation and Multiphase Flow Forum, presented at the 1990 Spring Meeting of the Fluids Engineering Division, held in conjunction with the 1990 Forum of the Canadian Society of Mechanical Engineers, University of Toronto, Toronto, Ontario,Canada, June 4-7, 1990*, FED-98, pages 153–158, 1990.

[3] Yves Dellanoy. *Modélisation d' écoulements instationnaires et cavitants*. PhD thesis, INPG Grenoble, 1989.

[4] J.P. Van Doormaal, G.D. Raithby, and B.H. McDonald. The segregated approach to predicting viscous compressible fluid flows. *ASME Journal of Turbomachinery*, 109:268–277, April 1987.

[5] F.H. Harlow and J.E. Welch. Numerical calculation of time-dependent viscous incompressible flow of fluid with free surface. *The Physics of Fluids*, 8:2182–2189, 1965.

[6] Francis H. Harlow and Anthony A. Amsden. Numerical calculation of almost incompressible flow. *Journal of Computational Physics*, 3:80–93, 1968.

[7] H.W.M. Hoeijmakers, M.E. Janssens, and W. Kwan. Numerical simulation of sheet cavitation. In J.M. Michel and H. Kato, editors, *Third International Symposium on Cavitation, April 7-10, 1998, Grenoble, France*, volume 2, pages 257–262, 1998.

[8] R. I. Issa. Solution of the implicitly discretised fluid flow equations by operator splitting. *Journal of Computational Physics*, 62:40–65, 1986.

[9] R.I. Issa and F.C. Lockwood. On the prediction of two-dimensional supersonic viscous interactions near walls. *AIAA Journal*, 15(2):182–188, February 1977.

[10] J.J.I.M. Van Kan. A second-order accurate pressure correction method for viscous incompressible flow. *SIAM J.SCi.Stat.Comp*, 7:870–891, 1986.

[11] K.C. Karki and S.V. Patankar. Pressure based calculation procedure for viscous flows at all speeds in arbitrary configurations. *AIAA journal*, 27(9):1167–1174, September 1989.

[12] P.K. Khosla and S.G. Rubin. A diagonally dominant second-order accurate implicit scheme. *Computers and Fluids*, 2:207–209, 1974.

[13] Charles L. Merkle, JinZhang Feng, and Phillip E.O. Buelow. Computational modelling of the dynamics of sheet cavitation. In J.M. Michel and H. Kato, editors, *Third International Symposium on Cavitation, April 7-10, 1998, Grenoble, France*, volume 2, pages 307–311, 1998.

[14] Jean-Luc Reboud, Benoit Stutz, and Olivier Coutier. Two-phase flow structure of cavitation: Experiment and modelling of unsteady effects. In J.M. Michel and H. Kato, editors, *Third International Symposium on Cavitation, April 7-10, 1998, Grenoble, France*, volume 2, pages 203–208, 1998.

[15] Byeong Rog Shin and Toshiaki Ikohagi. A numerical study of unsteady cavitating flows. In J.M. Michel and H. Kato, editors, *Third International Symposium on Cavitation*, volume 2, pages 301–306, 1998.

[16] W. Shyy and M.E. Braaten. Adaptive grid computations for inviscid compressible flows using a pressure correction method. AIAA Paper 88-3566-CP, 1988.

[17] Charles Song and Jianning He. Numerical simulation of cavitating flows by single-phase flow approach. In J.M. Michel and H. Kato, editors, *Third International Symposium on Cavitation, April 7-10, 1998, Grenoble, France*, volume 2, pages 295–300, 1998.

[18] D.R. van der Heul and P. Wesseling. A staggered scheme for hyperbolic conservation laws. In *Computational Fluid Dynamics '98, Proceedings of the Fourth ECCOMAS Computational Fluid Dynamics Conference, Athens, Greece, 7-11 September, 1998*, volume 1, pages 730–735. Wiley, 1998.

[19] Yiannis Ventikos and George Tzabiras. A numerical study of the steady and unsteady cavitation phenomenon around hydrofoils. In *International Symposium on Cavitation, CAV'95, May 1995, Deauville, France*, pages 441–448, 1995.

[20] P. Wesseling. Von Neumann stability conditions for the convection-diffusion equation. *IMA journal of Numerical Analysis*, 16:583–598, 1996.